J Sol-Gel Sci Technol (2015) 75:436–446
DOI 10.1007/s10971-015-3716-2

ORIGINAL PAPER

A new method for elaborating mesoporous SiO_2/montmorillonite composite materials

Tesnime Abou Khalil[1] · Semy Ben Chaabene[1] · Souhir Boujday[2,3] · Juliette Blanchard[2,3] · Latifa Bergaoui[1,4]

Received: 29 December 2014 / Accepted: 18 April 2015 / Published online: 25 April 2015

Abstract We report the sol–gel preparation of SiO_2/montmorillonite composite materials and the investigation of the effect of the amount of clay and the TEOS concentration on the textural and structural properties of the composites. Pre-swelling of the clay with cetyltrimethyl ammonium results in solids with a larger mesoporous surface area. A decrease in the gel time and an increase in the surface area were observed upon increasing the amount of clay in the reaction medium. These porous solids showed acidic properties, and their acidities were correlated with the amount of the clay mineral. The obtained composites were functionalized by adding manganese, and their catalytic properties were evaluated in the cyclohexene oxidation reaction.

Graphical Abstract

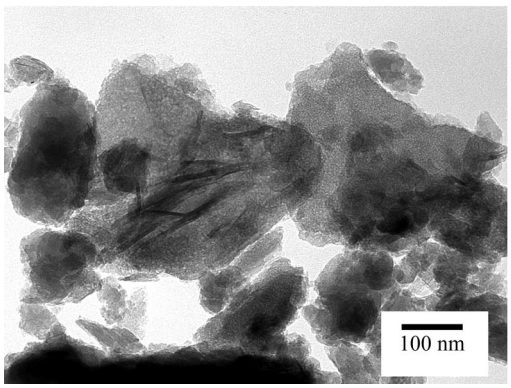

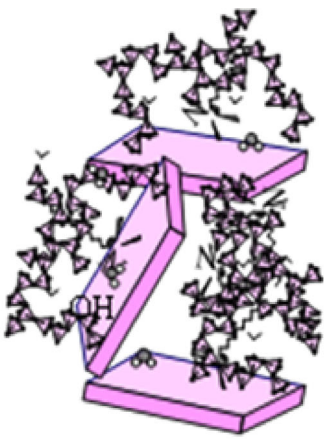

✉ Tesnime Abou Khalil
tttesnime@yahoo.fr

[1] Laboratoire de Chimie des Matériaux et Catalyse, Faculté des Sciences de Tunis, Université Tunis El Manar, Tunis, Tunisia

[2] Laboratoire de Réactivité de Surface, UMR CNRS 7197, Sorbonne Universités, UPMC Univ Paris 6, 75005 Paris, France

[3] Laboratoire de Réactivité de Surface, CNRS, UMR 7197, 75005 Paris, France

[4] Département de Génie biologique et Chimique, Institut National des Sciences Appliquées et de Technologie, Université de Carthage, Tunis, Tunisia

Keywords Clay modification · Silica · Sol–gel · Mesoporosity · Cyclohexene oxidation

1 Introduction

Smectite clay minerals have many advantages such as high cation exchange capacities and high swelling potentials [1]. Swelling can be used to allow access to the internal surface of the clay, but the collapse of the swollen layers upon drying results in the loss of this accessibility. This situation can be avoided by "pillaring" the clay layers, i.e., by the introduction of thermally stable pillars that prevent the interlayer spaces from collapsing and generate a two-dimensional porous material (PILC's) [2]. In this case, the inner surface of clay mineral layers remains accessible after calcination, making PILC's interesting solids for catalytic applications. Adsorption and catalysis studies on pillared clays have shown that the active sites arise mainly from the pillars [3, 4]. Our study on the acidity of clay intercalated with sulfated zirconia pillars [5] has shown that this material has possible applications in acid catalysis provided that the molecules involved are not too voluminous. Indeed, for several reactions, the narrow size of the interlayer space (in the microporous range) limits the diffusion of voluminous molecules to the active sites and is therefore responsible for the low activity of these catalysts. For this reason, the preparation of materials with a hierarchically structured porosity becomes an objective for applications in adsorption or catalysis.

To this end, we have developed, in the present work, a sol–gel method for preparing new SiO_2/clay composite materials. The sol–gel method has been extensively used for the preparation of a wide variety of materials with controlled pore size and surface area [6]. Mesoporous silica particles synthesis has often been reported using different organic molecules as template: organic acids [7], surfactants [8], amines [9] and sugars [10]. In nanotechnology, the preparation of clay/polymer nanocomposites is now a mature field of research. These hybrid materials often lead to superior performances over individual organic polymers or conventional filled composites [11]. In this work, we prepared clay/inorganic polymer nanocomposites, using tetraethoxysilane as the monomer and montmorillonite as the clay. The objectives of this study are (1) to investigate the effect of the clay mineral on the formation of the silica framework, (2) to examine the effect of the silica precursor on the delamination of the clay layers and (3) to search for a synergetic effect of the interaction between silica and clay layers on the porosity, acidity and catalytic activity. This approach is different from the one used for the porous clay heterostructures (PCH) preparation [12–14] which also involves sol–gel reactions and clay minerals. In the PCH preparation, smectite clay is swollen with a surfactant and the silica source is allowed to hydrolyze and condensate around the surfactant micelles, within the interlayer gallery. In this work, sodium and alkylammonium-exchanged montmorillonite were used, but, unlike the pillaring approach or PCH preparation, the sol–gel process leads to a silica network with random dispersion of clay layers (the goal being to increase the fraction of the mesoporous surface).

2 Experimental

2.1 Preparation of Na–montmorillonite

The clay used for this study is a Wyoming montmorillonite provided by the Source Clay Minerals Repository (University of Missouri, Columbia). The clay was sodium-saturated by three exchanges in 1 mol L^{-1} aqueous solutions of NaCl (4 g of clay mineral in 100 mL) and then washed until free of chloride ions. The size fraction below 2 μm was recovered by decantation and dried.

2.2 Preparation of CTMA–montmorillonite

Na–montmorillonite (2.5 g) was stirred with distilled water (250 mL) for 24 h. Cetyltrimethylammonium bromide (CTMAB; 1.15 g) was added to the suspension. The mixture was stirred for 3 h. The suspension was then treated in an ultrasonic bath for 1 h, washed until free of bromide ions, centrifuged and then dried overnight at 70 °C.

2.3 Synthesis of the SiO_2/clay composites

Solutions with different concentrations of TEOS in ethanol were prepared using 4 g of TEOS with variable ethanol volumes. A certain amount of Na–montmorillonite or CTMA–montmorillonite was added to the TEOS solution. After 24 h of stirring, 1.44 mL of 0.8 mol L^{-1} aqueous HCl solution was added to the suspension and the mixture was stirred at 70 °C under reflux until the formation of a gel. This gel was dried at 70 °C and calcined at 600 °C under oxygen for 3 h (heating rate 2 °C min^{-1}). Table 1 cites the conditions used for different preparations, where m is the mass (g) of clay mineral for 4 g of TEOS.

2.4 Catalysts preparation

During 1 h, 2 g of fumed silica (Sigma-Aldrich) or B_1 solid was stirred in 200 mL of distilled water. Then, 200 mL of manganese (II) perchlorate ($Mn(ClO_4)_2$ $6H_2O$) aqueous

Table 1 Experimental conditions of different prepared materials

Sample	[TEOS] (mol L^{-1})	$m_{organic\ montmorillonite}$ (g)	Sample	[TEOS] (mol L^{-1})	$m_{organic\ clay\ mineral}$ (g)
$A_{0.5}$	2	0.5	$B_{0.8}$	0.8	1.5
A_1		1	B_1	1	
			$B_{1.2}$	1.2	
$A_{1.5}$		1.5	$B_{1.4}$	1.4	
			$B_{1.6}$	1.6	
A_2		2	$B_{1.8}$	1.8	
			B_2	2	

Sample *N*: [TEOS] = 2 mol L^{-1} and $m_{Na–montmorillonite}$ = 1.5 g

Sample *S*: [TEOS] = 2 mol L^{-1} and $m_{montmorillonite}$ = 0 g

solutions with different concentrations (10^{-2}, 5×10^{-2} and 0.1 mol L^{-1}) was added to the suspension, which was stirred for 24 h. The pH values were below 4 for all suspensions. The solid phase was recovered by centrifugation, washed with 20 mL of distilled water, dried at room temperature and calcined under oxygen at 500 °C with a heating rate of 4 °C min^{-1}. Retained manganese was analyzed by X-ray fluorescence or after dissolution by ICP.

2.5 Characterization

BET surface area and pore size distributions were measured by N_2 adsorption/desorption at 77 K using a Micromeritics surface area analyzer (ASAP 2000). Prior to analysis, all samples were degassed at 200 °C under vacuum. The average pore diameters of the different samples were determined by the BJH method applied to the adsorption isotherm. The microporous surface area was evaluated using the *t*-plot method. FTIR measurements were taken with a PerkinElmer Spectrum XT infrared spectrometer using KBr pellets. The XRD patterns were obtained using a Philips PW 1730/10 X-ray diffractometer with CuKα radiation. Fluorescence measurements were taken on a Spectro XEPOS EDXRF and ICP measurements on a Horiba Jobin–Yvon (Activa) apparatus. Temperature-programmed desorption of ammonia (NH_3 TPD) was performed with a Micrometrics Autochem 2910 equipped with a thermal conductivity detector. The powdered samples (ca. 200 mg) were heated under He from RT to 600 °C at a rate of 1 °C min^{-1} and kept under He for 1 h. The temperature was then decreased to 150 °C under He, and 5 % NH_3/He was flushed on the sample for 30 min at this temperature. Afterward, loosely bonded NH_3 was removed by flowing He on the sample at 150 °C for 1 h. Desorbed NH_3 was observed from 150 to 600 °C. The morphologies of the solids were observed using a JEOL100CX transmission electron microscope (TEM).

2.6 Catalytic testing for cyclohexene oxidation reaction

The reactions were carried out at 40 °C under constant stirring in a 50-mL round-bottom flask equipped with a reflux condenser. The composition of the reaction medium was 0.25 mL of cyclohexene, 0.1 mL of toluene (internal standard), 5.0 mL of dichloromethane (solvent) and 0.1 g of the heterogeneous catalyst. Under nitrogen, 0.5 mL of t-BuOOH, the oxidizer, was added to the stirred solution. After 24 h, products were collected and analyzed by capillary gas chromatography (Agilent GC).

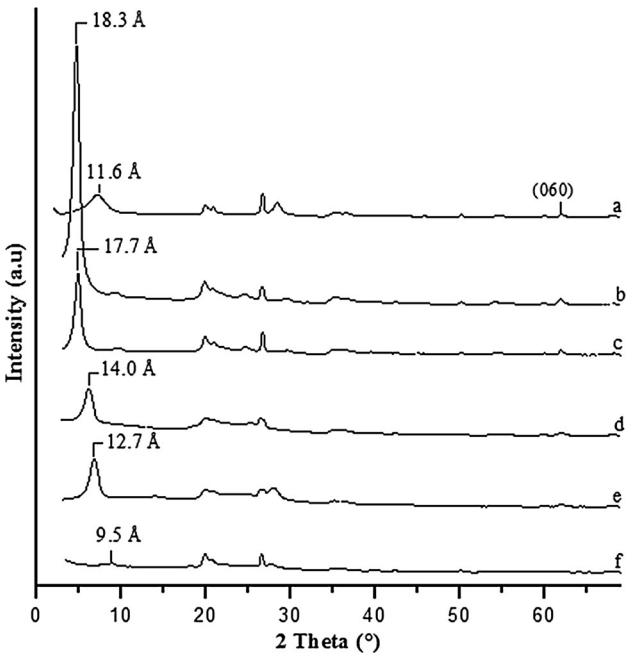

Fig. 1 XRD patterns of *a* Na–montmorillonite, *b* CTMA–montmorillonite, *c* $A_{1.5}$ before HCl addition, *d* $A_{1.5}$ after gelation, *e* *N* sample after gelation and *f* $A_{1.5}$ after calcinations at 600 °C

3 Results and discussion

3.1 X-ray diffraction

The X-ray diffraction patterns of Na–montmorillonite, CTMA–montmorillonite, $A_{1.5}$ before gel formation, *N* and $A_{1.5}$ after gel formation and $A_{1.5}$ after calcination are shown in Fig. 1. The basal spacing d_{001} of the Na–montmorillonite is 11.6 Å (Fig. 1a). As expected, the modification of the montmorillonite with cetyltrimethyl ammonium increases the d_{001} distance to 18.3 Å (Fig. 1b). According to surfactant arrangement models, this result matches the lateral-bilayer model [15, 16]. The solid obtained after stirring the mixture of TEOS and organic clay for 24 h (no HCl addition) shows a (001) reflexion at 17.7 Å (Fig. 1c). The presence of the TEOS molecules seems to only slightly change the distribution of $CTMA^+$ in the interlayer space. The peak at 17.7 Å disappears after addition of the HCl solution and formation of the gel, and a weaker peak is observed at 14 Å (Fig. 1d). The basal spacing of 14 Å might correspond to H^+–montmorillonite [17]. When the HCl solution was added to the CTMA–montmorillonite suspension, a partial $H^+/CTMA^+$ exchange may have taken place, inducing a partial collapse of the clay layers. This 14 Å basal spacing can also be attributed to CTMA–montmorillonite with the monolayer model [13, 14].

In any case, the disappearance of the intense and sharp d_{001} peaks at 18–17 Å shows that the well-stacked CTMA–montmorillonite layers have been drastically disturbed by the gel formation. This is probably the result of a disordered inorganic polymerization of TEOS entities between the montmorillonite layers. When Na–montmorillonite was used instead of CTMA–montmorillonite, the gel formation did not seem to disturb the stacking of the clay mineral since $d_{001} = 12.7$ Å (Fig. 1e), indicating a Na-smectite with one-water-layer hydration state [18].

Therefore, the presence of alkylammonium in the interlayer space improves the access of TEOS to the internal layer surface. The use of a pre-swelled clay mineral provides a better clay delamination. After calcination of the $A_{1.5}$ sample at 600 °C, a very weak peak at 9.5 Å remains (Fig. 1f). This peak likely corresponds to the thickness of the T-O-T layers. This allows us to conclude that the layer stacking that gave the peak at 14 Å before calcination collapses totally after calcination. This collapse is due to either the dehydration of the interlamellar space of the H^+–montmorillonite fraction or the total decomposition of interlamellar organic species. After calcination, the absence of the in-plane 060 reflection, around $2\theta = 60°$, characteristic of the clay mineral layer, suggests an important dehydroxylation of the clay layers.

The effect of the TEOS concentration on the structure of the prepared solids before and after calcination was examined by XRD (Fig. 2). The diffractograms of the seven samples are similar to those of $A_{1.5}$ with the d_{001} reflection located around 13.8 Å for dried solids and around 9.7 Å after calcination at 600 °C.

The effect of the amount of clay mineral was also investigated on samples prepared with constant TEOS concentration (2 mol L^{-1}). The intensity of the 001 reflection (Fig. 3), which can be associated with stacked (non-delaminated) layers, increases with the amount of CTMA–montmorillonite. The delamination would be more efficient when the clay mineral layers are better dispersed, resulting in lower d_{001} peak intensity.

3.2 Textural properties and gel time

The N_2 adsorption–desorption isotherms at 77 K of some of the calcined samples are shown in Fig. 4, and surface areas and gel times of prepared silica–clay composites are presented in Table 1.

The sample prepared without clay mineral (S) gives a type I isotherm with a H_4-type hysteresis (Fig. 4e), indicating that this sample is mainly microporous. BJH analysis of the adsorption curves confirms the presence of mesopores (average pore diameters between 41 and 57 Å) in all the samples containing CTMA–montmorillonite. The comparison of the isotherms reveals that the hysteresis loop grows larger when the amount of CTMA–montmorillonite increases (Fig. 4a–d).

This is indicative of an increase in the fraction of mesopores. Moreover, the comparison of $A_{1.5}$ (prepared from organic montmorillonite) and *N* (prepared from Na–montmorillonite) isotherms results (Fig. 4b, f, respectively) shows that the use of Na–montmorillonite (instead of CTMA–montmorillonite) dramatically decreases the overall surface area (81 $m^2\ g^{-1}$ for *N* sample compared to 360 $m^2\ g^{-1}$ for $A_{1.5}$ sample) and mesoporous surface area (35 $m^2\ g^{-1}$ for *N* compared to 103 $m^2\ g^{-1}$ for $A_{1.5}$). The BET surface area is very low (81 $m^2\ g^{-1}$), confirming the absence of clay mineral layer delamination. To stress the importance of the organic mineral clay in the mesoporosity formation, the pore size distributions of *N* and $A_{1.5}$ samples are shown in Fig. 5. This figure shows that the *N* sample is mainly microporous, while the $A_{1.5}$ sample gives a wide size distribution mesopores.

For a constant TEOS concentration (left part of Table 2), the total surface area tends to increase when the amount of CTMA–montmorillonite increases (except for sample A_2). The surface due to mesoporosity also increases with the amount of CTMA–montmorillonite. This shows the important role of clay layers in generating

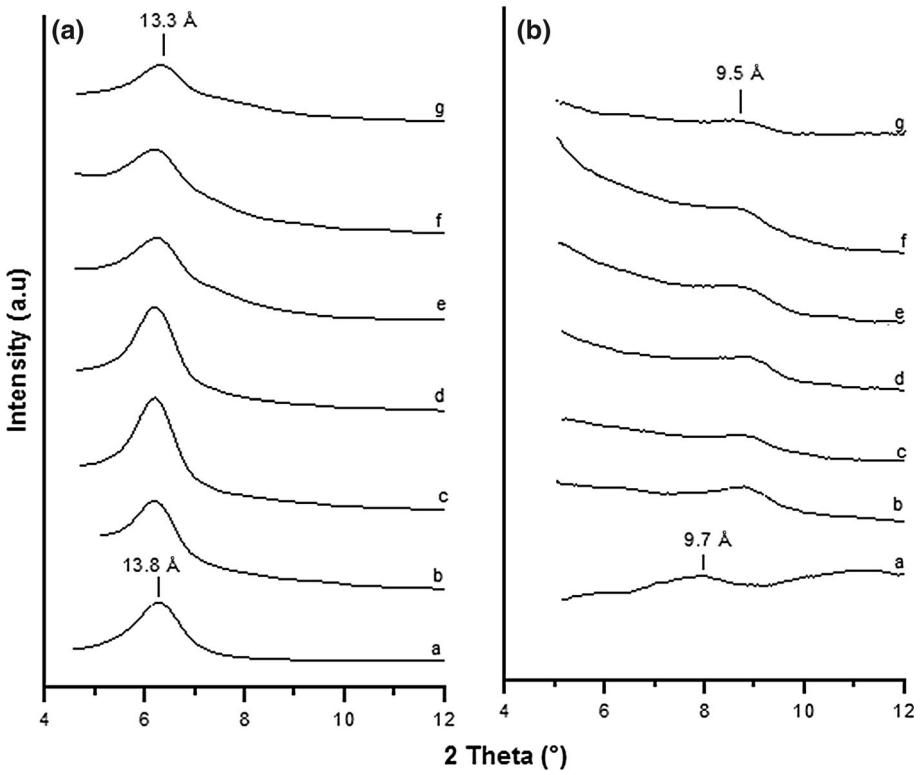

Fig. 2 XRD patterns of samples synthesized with a TEOS concentration equal to *a* 0.8, *b* 1.0, *c* 1.2, *d* 1.4, *e* 1.6, *f* 1.8 and *g* 2.0 mol L^{-1} (Table 1, series *B*); **a** before calcinations and **b** after calcinations at 600 °C

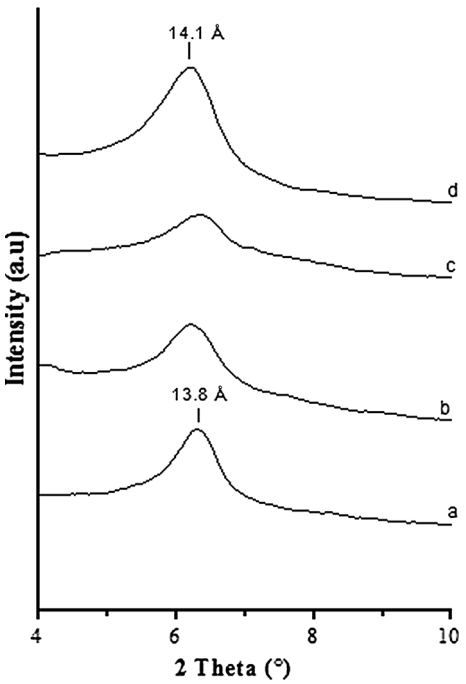

Fig. 3 XRD patterns of samples synthesized with an organic montmorillonite mass equal to *a* 0.5, *b* 1.0, *c* 1.5 and *d* 2.0 g (Table 1, series *A*)

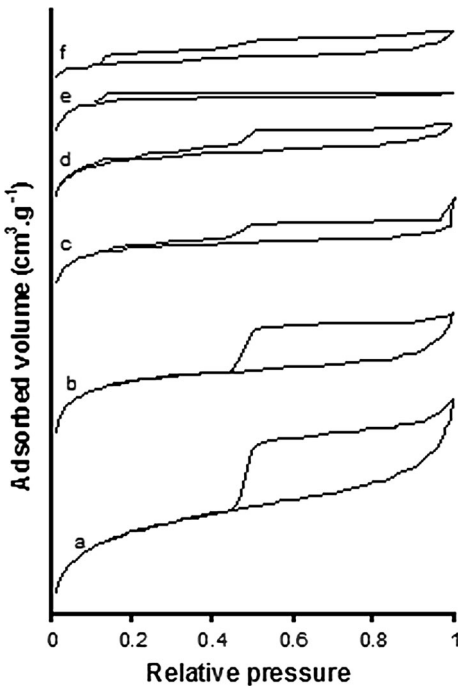

Fig. 4 N_2 adsorption–desorption isotherm of samples *a* A_2, *b* $A_{1.5}$, *c* A_1, *d* $A_{0.5}$, *e* *S*, and *f* *N* samples

mesoporosity. Table 2 also shows that, at constant TEOS concentration, the gel time decreases with the amount of CTMA–montmorillonite. Indeed, the gelation in the absence of CTMA–montmorillonite (*S*) requires 25 h. The gel time is barely modified by the addition of 1.5 g of Na–montmorillonite to the reaction medium (21 h for

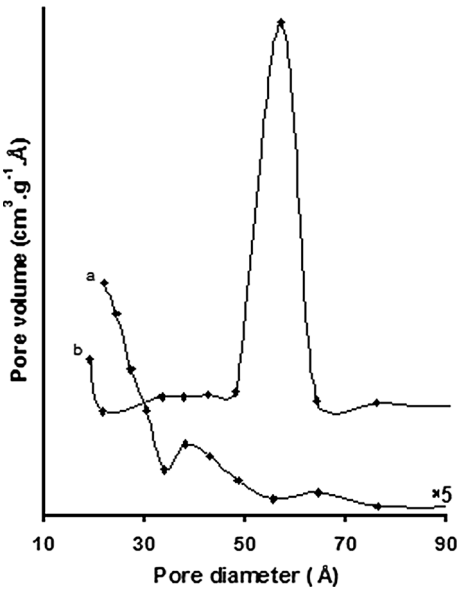

Fig. 5 Pore size distributions of *a* *N* and *b* $A_{1.5}$ samples

N sample). However, when the same mass of CTMA–montmorillonite is added, an important decrease in gel time is observed (5 h for $A_{1.5}$). This acceleration of the TEOS hydrolysis condensation kinetics in the presence of a surfactant has already been reported and assigned to the electrostatic interaction between the hydrophilic head groups of the surfactant molecules and the inorganic precursor [19, 20]. This important decrease in gel time could explain the generation of mesoporosity. In fact, it is known that the structure and the morphology of oxides depend greatly on the kinetics of the hydrolysis condensation reactions of the alkoxide [21]. However, the decrease in gel time is probably not the main factor responsible for the generated mesoporosity: The hydrolysis condensation of the fraction of the TEOS molecules located in the interlayer space of the clay can cause its delamination, thus generating mesoporosity. Regarding the decrease in the total surface area between $A_{1.5}$ and A_2, it should be reminded that the XRD study has shown an increase in the intensity of the (001) peak—and therefore of the fraction of stacked layers—upon increasing the CTMA–montmorillonite/TEOS ratio. This higher fraction of stacked layers is probably indicative of a lower extent of delamination and can account for the lower surface area. Therefore, to prepare a high surface area solid, CTMA–montmorillonite must be used, but high clay mineral concentrations should be avoided to ensure a high dispersion of the layers. The best condition seems to be attained for a CTMA–montmorillonite/TEOS weight ratio of 1.5/4. It is the reason why, for the study of the TEOS concentration effect, the amount of CTMA–montmorillonite was fixed at 1.5. The gel times and the surface areas of the prepared solids are presented in Table 2 (right part). The decrease in the TEOS concentration from 2 to 0.8 mol L^{-1} leads, as expected, to an important increase in gel time, since the condensation reaction rate is proportional to the TEOS concentration. The overall surface area, as well as the mesoporous surface area, tends to increase when the TEOS concentration decreases, confirming the importance of TEOS and CTMA–montmorillonite interactions in generating mesoporosity and that the slowing down of condensation reactions has no consequences on the extent of the delamination.

3.3 FTIR spectroscopy

IR spectroscopy was used to investigate the structural changes caused by the thermal treatment. Figure 6 shows the FTIR spectra of the CTMA–montmorillonite, the calcined $A_{1.5}$ and S samples. For the CTMA–montmorillonite, the bands at 461, 525, 616 and 910 cm^{-1} can be attributed to the Si–O bending, Al–O stretching, Al–OH and Al–OH–Al bending, respectively [22]. The bands at 780 cm^{-1} are related to vibrations of tetrahedral SiO_4 [23], and those at 1030 cm^{-1} are assigned to Si–O stretching [24]. The stretching vibrations of CH_2 groups at 2918 and 2847 cm^{-1} and the bending of CH_3 and CH_2 at about 1480 cm^{-1} are assigned to the intercalated alkylammonium species [25]. The two bands at 3434 and 1625 cm^{-1} correspond to water molecule vibrations. Finally, the band at 3620 cm^{-1} is assigned to the vibration of structural OH groups linked to ^{VI}Al. After calcination, no bands attributable to organic

Table 2 BET area (S_{BET}), mesoporous surfaces (S_{meso}) and gel time (t_g) of different prepared samples

Sample	S_{BET} (m^2 g^{-1})	S^a_{meso} (m^2 g^{-1})	t_g (h)	Sample	S_{BET} (m^2 g^{-1})	S^a_{meso} (m^2 g^{-1})	t_g (h)
N	81	35	21	$B_{0.8}$	469	172	216
S	286	46	25	B_1	381	184	120
$A_{0.5}$	257	77	24	$B_{1.2}$	396	128	72
A_1	297	86	7	$B_{1.4}$	361	108	41
$A_{1.5}$	360	103	5	$B_{1.6}$	372	95	24
A_2	317	173	4	$B_{1.8}$	355	83	9
				B_2	360	103	5

[a] $S_{mesoporous} = S_{BET} - S_{microporous}$, since the external surface area can be neglected

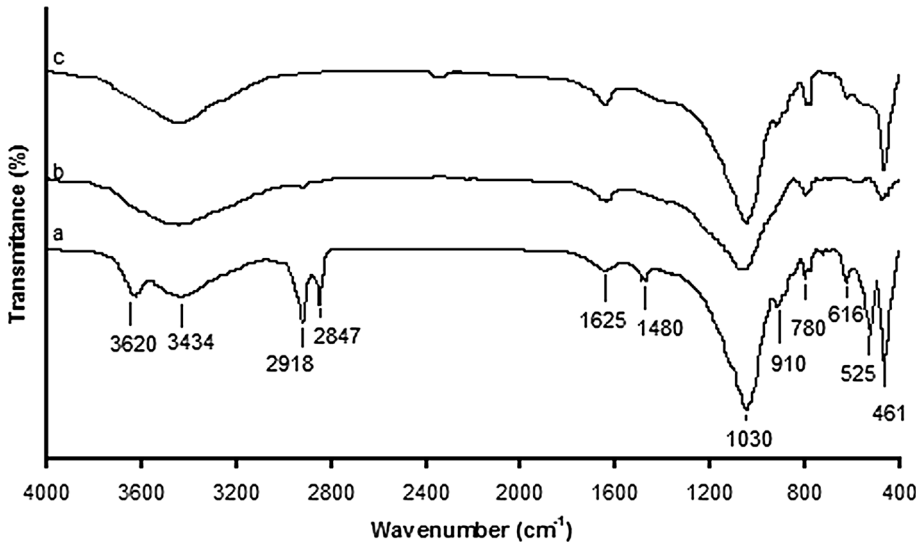

Fig. 6 FTIR spectrum of *a* CTMA–montmorillonite, *b* $A_{1.5}$ and *c* *S* samples

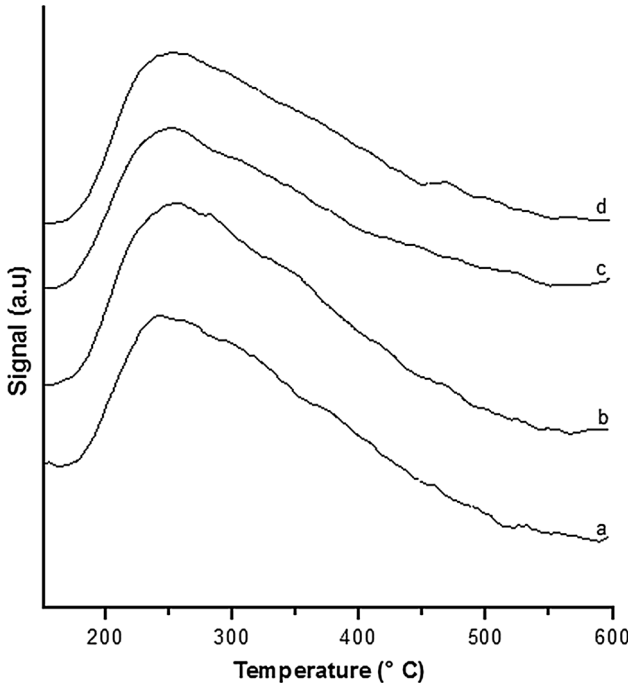

Fig. 7 NH_3 TPD profiles of samples synthesized with an organic montmorillonite mass equal to *a* 0.5, *b* 1.0, *c* 1.5 and *d* 2.0 g (Table 1, series *A*)

groups remain (Fig. 6b), evidence of the decomposition and elimination of the organic matter. The enlargement of the intense peak near 1030 cm^{-1}, assigned to Si–O stretching vibrations, can be ascribed to the formation of new silica species in addition to the tetrahedral SiO_4 related to clay mineral. Besides, the band assigned to structural OH groups vibration (3620 cm^{-1}) is absent after calcination, indicating the destruction of the montmorillonite layer structure. This fact was observed by Li et al. [26] and attributed to a strong interaction between the amorphous silica and the octahedral aluminum in montmorillonite layers. After calcination, the $A_{1.5}$ spectrum is closer to the SiO_2 spectrum (Fig. 6c) than to a clay mineral spectrum.

3.4 NH_3 TPD

NH_3 TPD profiles of the solids prepared with different amounts of CTMA–montmorillonite show similar shapes (Fig. 7) with a broad NH_3 desorption peak between 200 and 500 °C. The maximum at ca. 250 °C indicates that these samples mainly contain mild acid sites similar to those found in mesoporous aluminosilicates [27]. The tailing toward higher desorption temperatures indicates that stronger acid sites are also present. From a quantitative point of view, stress should be laid on the slight increase in the acid site concentration with the amount of CTMA–montmorillonite. Indeed, the acid site concentrations are 34, 42, 42 and 47 μmol g^{-1} for $A_{0.5}$, A_1, $A_{1.5}$ and A_2 calcined samples, respectively. This result is not only a confirmation that the clay is at the origin of the acidity, but also an indication that the number of acid sites is not proportional to the amount of clay in the sample. This is consistent with the fact that the extent of delamination (and hence the fraction of the internal surface of the clay that becomes accessible) decreases when the amount of clay increases.

3.5 Transmission electron microscope

TEM images of calcined B_1 are shown in Fig. 8. The three TEM micrographs show the presence of clay mineral layers dispersed inside a silica matrix. In Fig. 8a, stacked layers can be clearly observed and the d-spacing estimated from

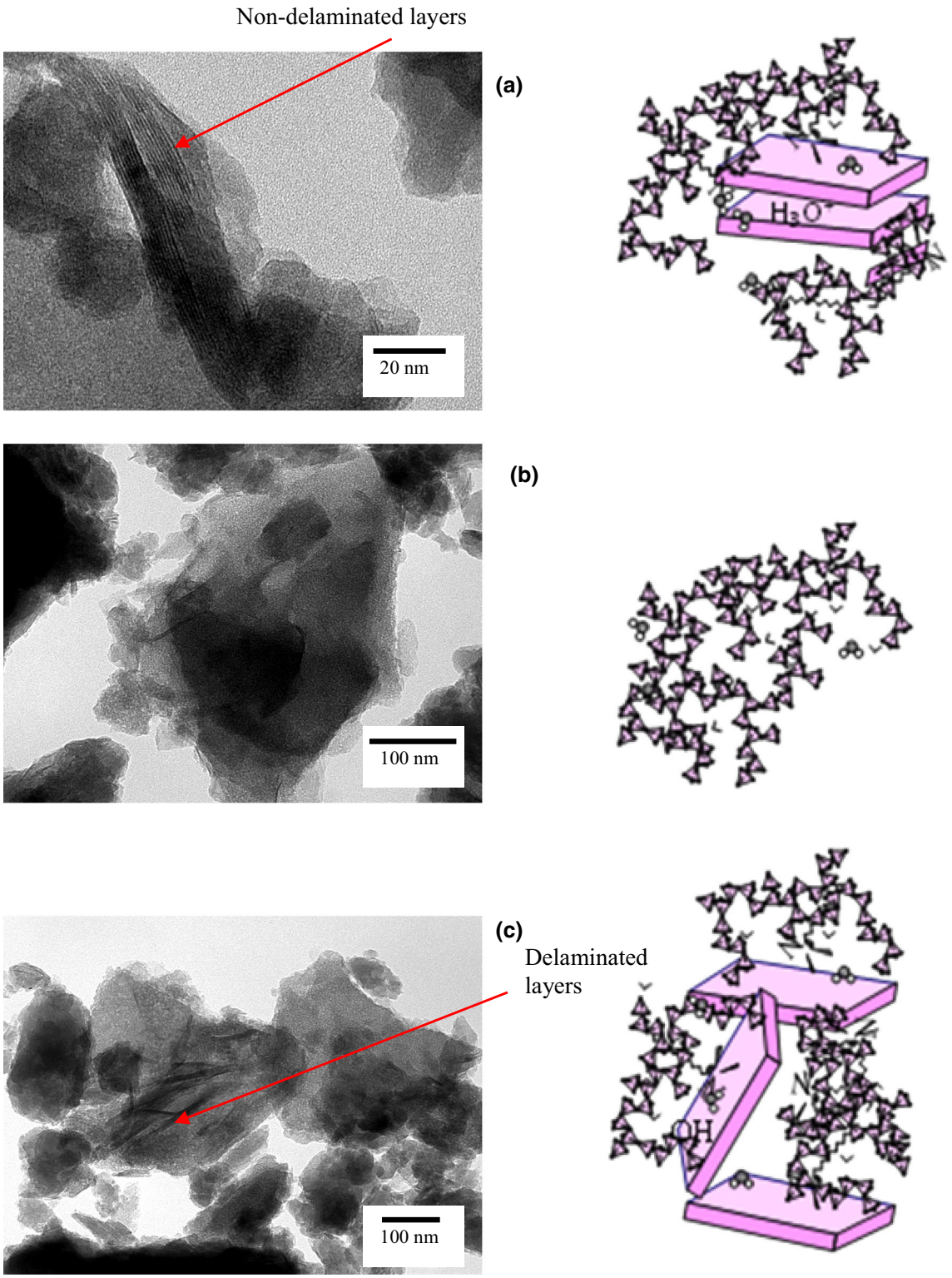

Fig. 8 TEM images of the B_1 sample after calcinations and possible structure model after gelation of clay/TEOS mixture

TEM (9.6 Å) matches the basal spacing obtained from the XRD pattern of the calcined sample (9.5 Å, Fig. 1f). Figure 8b, c shows delaminated clay layers and some silica particles that do not contain clay minerals. The possible structural models of the composite materials are illustrated in Fig. 8. Polymerized SiO_2 (Fig. 8b), with no interaction

Table 3 Cyclohexene conversions and selectivities of silicate and nanocomposite samples for different amounts of retained manganese

Catalyst	$[Mn^{2+}]$ in the solution (mol L^{-1})	Mn (wt%)	Conversion (%)	Selectivity (%)			
				P_1	P_2	P_3	P_4
S	10^{-2}	0.08	19.4	24.6	55.8	5.2	14.4
	5×10^{-2}	0.52	42.1	32.9	44.6	2.2	20.3
	0.1	0.99	69.5	29.8	36.4	3.4	30.4
B	10^{-2}	0.15	28.0	50.2	35.4	0	14.4
	5×10^{-2}	1.04	15.6	63.1	36.9	0	0
	0.1	1.58	20.6	56.1	43. 9	0	0

P_1, 2-cyclohexene-1-ol; P_2, 2-cyclohexene-1-one; P_3, cyclohexene oxide; P_4, cyclohexane diols

with clay layers, might be responsible for the microporosity detected in the material after calcinations (non-delaminated layers (Fig. 8a) do not develop a significant surface area since the interlayer space is mostly inaccessible to N_2). On the other hand, during polymerization, the interaction of TEOS with clay layers will possibly provide mesoporosity (Fig. 8c). Formation of microporous silica domains free of clay layers and of composites domains responsible for the mesoporosity occurs most probably in all samples but to a different extent depending on experimental conditions, and this, results in the variation of the fraction of mesopores in the samples.

3.6 Epoxidation of cyclohexene

As expected, the amount of retained manganese is proportional to the Mn^{2+} concentration in the used solution for the catalysts functionalization (Table 3). The manganese is most likely retained through an adsorption mechanism since the clay mineral layers lost their cationic exchange capacity in the composite after calcination.

Previous works on the oxidation of cyclohexene by t-BuOOH (TBHP) in the presence of Ti, V, Cr and Mo complexes [28] showed that the O–O bond of peroxide can be broken by two competing reactions. The first is a heterolytic cleavage that leads to cyclohexene oxide. When combined with water, this oxide gives cyclohexane-1,2-diol [29]. The second is a homolytic cleavage that leads to radical reactions and produces cyclohexen-1-ol and cyclohexen-1-one [30–33]. Cyclohexene has a very high affinity for radicals. Indeed, it is easy to extract allylic hydrogen [34–37], because the carbon–hydrogen bond in α position of the double bond and the oxygen–hydrogen bond of hydroperoxide have similar energies. Besides, for the oxidation of cyclohexene in the presence of Mn–zeolite, it has been shown that ROOH decomposition on Mn centers is a kinetically relevant step. In fact, the oxidation rate on Mn–zeolite is first order in [ROOH] and proportional to the number of redox-active Mn sites [38]. The intent of our study was not to reach a very high conversion or an important selectivity for one of the products of the reaction, but rather to use the cyclohexene oxidation reaction to explore the accessibility of Mn sites to TBHP. Fumed silica was used for comparison to assess the 100 % accessibility because these particles are non-porous and have a surface area of 390 $m^2\ g^{-1}$, close to that of the B_1 sample. Cyclohexene conversions and selectivities for different amounts of Mn are presented in Table 3. First, it can be observed that Mn–fumed silica catalysts lead to higher conversions and are therefore more active than composite catalysts for comparable amounts of manganese. Moreover, values in Table 3 show that the cyclohexene conversion increases linearly with the amount of Mn at the surface of the fumed silica, while this is not true for the composite catalysts. The manganese at the surface of SiO_2/clay composite seems to be either not well dispersed or not fully accessible to TBHP molecules. This last hypothesis is consistent with the presence of micropores in the composites (in B_1 sample, mesopores account for <50 % of the overall surface). For Mn–fumed silica, the combined cyclohexene oxide and cyclohexane-1,2-diol selectivities are proportional to Mn amount and reach 34 %. The two parallel transformation pathways (allylic oxidation and epoxidation) seem to take place on Mn–fumed silica. However, for composites, it is clear that under the mentioned reaction conditions, the allylic oxidation pathway is virtually the only one that operates [39]. This may be due to the acidic sites present in B_1. In fact, it was observed that the TBHP promotes the allylic oxidation pathway when an acidic solid, such as alumina, is used as support for the transition metal ions [36, 40].

4 Conclusions

In this work, micro- and mesoporous materials were prepared by the gelation of alkoxysilane in the presence of montmorillonite. The gelation kinetics depends, obviously, on the TEOS concentration, but also greatly on the amount of organic montmorillonite in the synthesis medium. This

dependence is most likely related to the alkylammonium interfoliar cations, which play an important catalytic role. In addition to the SiO_2 microporosity, the presence of clay layers induces the formation of some mesoporosity. The mesoporosity is probably created during silica polymerization by inducing the clay mineral delamination. When the delamination is effective, the sample is likely comprised of clay layers dispersed inside a silica matrix structure. After calcination, a significant transformation of the montmorillonite layer structure takes place. The surface acidity of the resulting solids seems to be related to the presence of clay mineral. After functionalization with manganese, the catalysts were tested in the cyclohexene oxidation reaction by TBHP. The acidity of the solid seems to be high enough to promote the allylic oxidation pathway and to minimize the epoxide formation. On the other hand, not all of the Mn sites seem to be accessible to TBHP during the oxidation reaction.

References

1. Murray HH (2000) Traditional and new application for kaolin, smectite, and palygorskite: a general over view. Appl Clay Sci 17:207–221
2. Pinnavaia TJ, Tzou M-S, Landau SD, Raythatha RH (1984) On the pillared and delamination of smectite clay catalysis by polyoxo cations of aluminium. J Mol Catal 27:195–212
3. Lambert JF, Poncelet G (1997) Acidity in pillared clays: origin and catalytic manifestations. Top Catal 4:43–56
4. Vaccari A (1999) Clays and catalysis: a promising future. Appl Clay Sci 14:161–198
5. Ben Chaabene S, Bergaoui L, Ghorbel A, Lambert JF, Grange P (2003) Acidic properties of a clay prepared from the reaction of zirconyl chloride solution containing sulfate ions with montmorillonite. Appl Catal A-Gen 252:411–419
6. Sadek OM, Reda SM, Al-Bilali RK (2013) Preparation and characterization of silica and clay–silica core-shell nanoparticles using sol–gel method. Adv Nanoparticles 2:165–175
7. Dudarko OA, Gunathilake C, Sliesarenko VV, Zub YL, Jaroniec M (2014) Microwave-assisted and conventional hydrothermal synthesis of ordered mesoporous silicas with P-containing functionalities. Colloids Surf A 459:4–10
8. Zhao D, Huo Q, Feng J, Chmelka BF, Stucky GD (1998) Nonionic triblock and star diblock copolymer and oligomeric surfactant syntheses of highly ordered, hydrothermally stable, mesoporous silica structures. J Am Chem Soc 120:6024–6036
9. El-Toni AM, Habila MA, Ibrahim MA, Labis JP, Al Othman ZA (2014) Simple and facile synthesis of amino functionalized hollow core–mesoporous shell silica spheres using anionic surfactant for Pb(II), Cd(II), and Zn(II) adsorption and recovery. Chem Eng J 251:441–451
10. Rahman MS, Ambati J, Joshi S, Rankin SE (2014) Incorporation of isolated Ti sites into mesoporous silica thin films by sugar surfactant complexation. Micro Meso Mater 190:74–83
11. Ganguly SC (2001) Book review: polymer–clay nanocomposites in polymer science. In Pinnavaia TJ, Beall GW (eds) John Wiley & Sons Ltd., Chichester, West Sussex 370 pp. J Inorg Organomet Polym 11: 247–251
12. Galarneau A, Barodawalla A, Pinnavaia TJ (1994) Porous clay heterostructures formed by gallery-templated synthesis. Nature 374:529–531
13. Mercier L, Pinnavaia TJ (1998) A functionalized porous clay heterostructure for heavy metal ion (Hg^{2+}) trapping. Micro Meso Mater 20:101–106
14. Zhu HY, Ding Z, Lu CQ, Lu GQ (2002) Molecular engineered porous clays using surfactants. Appl Clay Sci 20:165–175
15. Lagaly G, Dékany I (2005) Adsorption on hydrophobized surfaces: clusters and self-organization. Adv Colloid Interface 114–115:189–204
16. Zhu JX, He HP, Guo JG, Yang D, Xie XD (2003) Arrangement models of alkylammonium cations in the interlayer of $HDTMA^+$ pillared montmorillonites. Chin Sci Bull 48:368–372
17. Aliouane N, Hammouche A, De Doncker RW, Telli L, Boutahala M, Brahimi B (2002) Investigation of hydration and protonic conductivity of H-montmorillonite. Solid State Ionics 148:103–110
18. Bérend I, Cases JM, Francois M, Uriot JP, Michot L, Masion A, Thomas F (1995) Mechanism of adsorption and desorption of water vapor by homoionic montmorillonites: 2. The Li^+, Na^+, K^+, Rb^+, and Cs^+-exchanged forms. Clay Clay Miner 43:324–336
19. Monnier A, Schüth F, Huo Q, Kumar D, Margolese D, Maxwell RS, Stucky GD, Krishnamurthy M, Petroff P, Firouzi A, Janicke M, Chmelka BF (1993) Cooperative Formation of inorganic–organic interfaces in the synthesis of silicate mesostructures. Science 261:1299–1303
20. Chen CY, Burkett SL, Li HX, Davis ME (1993) Studies on mesoporous materials II. Synthesis mechanism of MCM-41. Microporous Mater 2:27–34
21. Livage J, Henry M, Sanchez C (1988) Sol–gel chemistry of transition metal oxides. Prog Solid State Chem 18:259–341
22. Zhou CH, Li XN, Ge ZH, Li QW, Tong DS (2004) Synthesis and acid catalysis of nanoporous silica/alumina-clay composites. Catal Today 93–95:607–613
23. Zapata PA, Belver C, Quijada R, Aranda P, Ruiz-Hitzky E (2013) Silica/clay organo-heterostructures to promote polyethylene-clay nanocomposites by in situ polymerization. Appl Catal A 453:142–150
24. Li B, Mao H, Li X, Ma W, Liu Z (2009) Synthesis of mesoporous silica-pillared clay by intragallery ammonia-catalyzed hydrolysis of tetraethoxysilane using quaternary ammonium surfactants as gallery templates. J Colloid Interface Sci 336:244–249
25. Fatimah I, Huda T (2013) Preparation of cetyltrimethylammonium intercalated Indonesian montmorillonite for adsorption of toluene. Appl Clay Sci 74:115–120
26. Li F, Jiang Y, Xia M, Sun M, Xue B, Ren XA (2010) Novel mesoporous silica–clay composite and its thermal and hydrothermal stabilities. J Porous Mater 17:217–223
27. Tayade KN, Mishra M (2014) Catalytic activity of MCM-41 and Al grafted MCM-41 for oxidative self and cross coupling of amines. J Mol Catal A Chem 382:114–125
28. Arzoumanian H, Blanc A, Hartig U, Metzger J (1974) Homogeneous bimetallic catalysis. The selective autoxidation of cyclohexene. Tetrahedron Lett 12:1011–1014
29. Sakthivel A, Dapurkar SE, Selvam P (2003) Allylic oxidation of cyclohexene over chromium containing mesoporous molecular sieves. Appl Catal A 246:283–293
30. Mukherjee S, Samanta S, Bhaumik A, Ray BC (2006) Mechanistic study of cyclohexene oxidation and its use in modification of industrial waste organics. Appl Catal B Environ 68:12–20
31. Jermy BR, Kim SY, Bineesh KV, Selvaraj M, Park DW (2009) Easy route for the synthesis of Fe–SBA-16 at weak acidity and its

catalytic activity in the oxidation of cyclohexene. Micro Meso Mater 121:103–113
32. Tong J, Zhang Y, Li Z, Xia C (2006) Highly effective catalysts of natural polymer supported Salophen Mn(III) complexes for aerobic oxidation of cyclohexene. J Mol Catal A Chem 249:47–52
33. Ameur N, Bedrane S, Bachir R, Choukchou-Braham A (2013) Influence of nanoparticles oxidation state in gold based catalysts on the product selectivity in liquid phase oxidation of cyclohexene. J Mol Catal A Chem 374–375:1–6
34. Salavati Niassari M, Farzaneh F, Ghandi M, Turkian L (2000) Oxidation of cyclohexene with *tert*-butylhydroperoxide catalyzed by manganese(II) complexes included in zeolite Y. J Mol Catal A Chem 157:183–188
35. Salavati-Niasari M, Salemi P, Davar F (2005) Oxidation of cyclohexene with Tert-butylhydroperoxide and hydrogen peroxide catalysted by Cu(II), Ni(II), Co(II) and Mn(II) complexes of *N*,*N*′-bis-(α-methylsalicylidene)-2,2-dimethylpropane-1,3-diamine, supported on alumina. J Mol Catal A Chem 238:215–222
36. Habibi D, Faraji AR, Arshadi M, Fierro JLG (2013) Characterization and catalytic activity of a novel Fe nano-catalyst as efficient heterogeneous catalyst for selective oxidation of ethylbenzene, cyclohexene, and benzylalcohol. J Mol Catal A Chem 372:90–99
37. Sheldon RA, Kochi JK (1981) Metal-catalyzed oxidations of organic compounds. Academic Press, New York
38. Modén B, Zhan BZ, Dakka J, Santiesteban JG, Iglesia E (2006) Kinetics and mechanism of cyclohexane oxidation on MnAPO-5 catalysts. J Catal 239:390–401
39. Salavati-Niasari M (2008) Host (nanopores of zeolite-Y)/guest [manganese(II) with 12-membered tetradentate N_2O_2, N_2S_2 and N_4 donor macrocyclic ligands] nanocatalysts: flexible ligand synthesis, characterization and catalytic activity. Transit Metal Chem 33:443–452
40. Gemeay AH, Salem MA, Salem IA (1996) Activity of silica–alumina surface modified with some transition metal ions. Colloids Surf A 117:245–252